

An Eulerian-Lagrangian Computational Model for Deflagration and Detonation of High Explosives

Joseph R. Peterson, Charles A. Wight^{1,*}

Department of Chemistry, University of Utah, Salt Lake City, UT 84112 USA

Abstract

A solid phase explosives deflagration and detonation model capable of surface burning, convective bulk burning and detonation is formulated in the context of Eulerian-Lagrangian material mechanics. Well-validated combustion and detonation models, WSB and JWL++, are combined with two simple, experimentally indicated transition thresholds partitioning the three reaction regimes. Standard experiments are simulated, including the Aluminum Flyer Plate test, the Cylinder test, the Rate Stick test and the Steven test in order to validate the model. Cell and particle resolution dependence of simulation metrics are presented and global uncertainties assigned. Error quantification comparisons with experiments led to values generally below 7% (1σ). Finally, gas flow through porous media is implicated as the driving force behind the deflagration to detonation transition.

Keywords: Deflagration, detonation, Steven test, ViscoSCRAM, WSB, JWL++

1. Introduction

Deflagration to detonation transition (DDT) is a phenomenon studied in hazard mitigation due to a number of accidental explosions resulting from slow heating, low velocity impact or shock. These scenarios are classified as slow cook-off, unknown detonation transition (XDT), and shock detonation transition (SDT) based on their reaction violence, which depends on such things as heating rate, shock pressure, material porosity (age/density and quality/damage) and device geometry [1, 2]. Any model built for studying explosion accidents must accurately predict thermal reaction at various pressures and temperatures, the rate of bulk burning through the explosive medium in situations where damage may be present, and most importantly, the correct physics and mechanics for all materials in both low and high deformation regimes. The

*Corresponding Author:
Department of Chemistry
University of Utah
315 S. 1400 East, RM 2020
Salt Lake City, UT 84112-0850
Phone: 801-581-8796
Fax: 801-585-6749

Email address: chuck.wight@utah.edu (Charles A. Wight)

DDT model described in this paper (hereafter, DDT1) was designed and implemented with these criteria in mind in an attempt to model on the bulk a transition from low deflagration rates to high detonation rates.

DDT1 is the first multimaterial, multiphase DDT model implemented in the Uintah Computational Framework (UCF). It has the capability of running on massively parallel computer architectures with near ideal scalability up to approximately 10^5 cores allowing for simulation from simple to complex problems [3]. Capabilities of the model include correct detonation and SDT behavior for high velocity impact, go/no-go reactive behavior for low velocity impact and correct burning behavior during thermal decomposition. A previously reported 3D implementation of the WSB model for thermal decomposition and reaction of near ideal explosives is used for reacting in thermal decomposition and shock induced reaction modes of explosion [4, 5]. Detonation reaction is modeled with a modified version of JWLL++, a reactive flow model by Souers et al [6]. Two thresholds for transition between the three reaction regimes have been identified and implemented, one based on damage of the reacting material, and the other based on the equilibrium pressure in the explosive. Little or no experimental data from which these thresholds may be derived exist for many explosives. PBX 9501 was selected as the benchmark high energy (HE) material because an ample number of quantitative experiments in the convective burning regime have been reported, as well as large amounts of detonation and SDT data, but most importantly because data for these thresholds are available.

However, modeling explosive phenomena is complex. Processes such as hot spot formation, frictional heat dissipation during crack coalescence and separation, shear heating through plastic flow burning in porous materials and at grain/binder interfaces, which are all extremely important factors leading to DDT, cannot yet be modeled on the bulk. In an attempt to design a bulk model for deflagration and detonation, some necessary physics must be approximated. To this end, we combine two simple reaction models within a general physics framework in an attempt to capture many of the essential elements in the transition at high strain rates.

UCF is an appropriate choice for a computational framework because it contains implementations of Eulerian and Lagrangian materials, both of which are necessary for implementation of the WSB and JWLL++ models. Furthermore, it supports a large selection of equations of state for Eulerian materials and constitutive models for Lagrangian materials. All models are linked via an underlying multimaterial, multiphase physics implementation called MPMICE [7]. Many of the physical processes of DDT such as shock wave convergence, shock compression and heating, and near-TMD plug formation occur naturally as a result of implementing DDT1 in MPMICE. The massively parallel nature of UCF and recent advancements in scalability make it suitable for PetaScale problems such as predicting outcomes of large explosions [8, 9].

Following is a detailed description of the methodology adopted for the study, including a deeper discussion of UCF and model development. Descriptions of the material models, equations of state and reaction models are presented. Following the model descriptions, results for convective burning, including surface burning and bulk burning are presented, along with explosive properties of the model. These explosive properties

include SDT distances, rate stick failure data, and cylinder expansion data.

2. Simulation Methodology

Uintah Computational Framework¹ is used as the underlying framework into which the DDT1 was implemented. The model fits into a category of models designated “high energetic” (HE) reaction models. UCF includes model types such as constitutive models, reaction models, equations of state and component models, all of which are used in the study. Component models are such things as implicit continuous-fluid Eulerian (ICE) [10] or material point method (MPM) [11], in which the basic physics of a system are solved. ICE is a cell centered model in which a grid cell owns various thermodynamic properties including pressure which is calculated via an iterative pressure solve, volume and temperature as well as kinetic properties such as velocity. MPM is a particle model consisting of Lagrangian points, implemented as a quasi-meshless code in UCF. The GIMP particle-to-grid interpolator was chosen for its accuracy to performance ratio [12, 13]. DDT1 requires both MPM materials and ICE materials and as such is implemented in the MPMICE component. A variety of explosive scenarios have already been simulated successfully with the MPMICE component [7].

The model interface in UCF is designed to allow each model to modify data, usually as “sources” or “sinks”. For example, in material models sources and sinks manifest as deformation and stresses. Because DDT1 is a reaction model, it computes sources and sinks for mass (from one material to another) and energy (representing exothermic or endothermic reactions). Implementing a reaction model in UCF entails solving appropriate rate equations for the reactions and ensuring that conservation laws are obeyed. A parallel task graph ensures that tasks are executed in the correct order to make necessary data available to each module in a consistent manner and that the material physics are modeled by the simulation component.

The plug-and-play style model interface employed by UCF allows for a high degree of complexity in problem formulation, while at the same time facilitating fast prototyping of new simulations. Once a good setup is found, activating more advanced models entails implementing sources/sinks, writing an input specification and adding the input parameters to the input file. Using a material model already implemented merely requires having correct input parameters. For example steel, copper and aluminum already have well validated hypo-elastic behavior and parameterization [14]. Each validation simulation performed herein went through a variety of stages, consisting of more complexity with each iteration and as a consequence an increasing amount of computational resources. The following subsections describe the models used for the final validation experiments.

Of particular importance to modeling is understanding the spatial resolution dependences of the various fundamental metrics of interest. Since MPMICE has both particle resolution, the number of particles in each

¹<http://www.uintah.utah.edu>

direction in each cell, and cell resolution, studies over both convergence spaces are required. Quantification of resolution dependences allows assignment of reasonable uncertainty outside the ranges of model calibration. Resolution studies were performed for all simulated observables, including detonation velocity, deflagration velocity, Chapman-Jouguet (CJ) pressure and case expansion velocities.

2.1. Equations of State

Three equations of state (EOS) were used for representing the HE reactant and product states. Two of these are JWL equations, $p = A \exp(-R_1 v) + B \exp(-R_2 v) + \omega C_v T/v$, the standard equation of state chosen for SDT simulations by a number of scientific groups [15, 6, 16]. The JWL EOS takes the specific volume, v , the temperature, T , and specific heat, C_v , as well as five fitting parameters, A , B , R_1 , R_2 and ω and calculates the bulk average pressure. Numerous fits for product and reactant materials are available in literature, most of which have standardized R_1 , R_2 and ω parameters, making the use of the JWL EOS efficient from a standpoint of quick turnaround time for a scenario prototyped with a different explosive material. EOS parameters for detonation products and reactant behavior of PBX 9501 were taken from Table 3 of Vandersall et al [17].

A second product equation of state is necessary for representing products from surface and bulk burning, as they have fundamentally different behavior than detonation products. The TST equation of state, $p = (\gamma - 1)C_v T/(v - b) - a/(v + 3.0b)(v - 0.5b)$, was used for its particularly good representation of species relevant to combustion (i.e. CO₂, N₂, H₂O) [18]. Parameters used for product gases are $a = -260.1 \text{ Pa m}^3$, $b = 7.955 \times 10^{-4} \text{ m}^3$ and $\gamma = 1.63$. Variable v , T and C_v are the specific volume, temperature and specific heat respectively.

Mass and energy is either transferred to the burn products or detonation products depending on the mode of combustion. Surface burning and bulk burning products were represented by the TST EOS and detonation products were represented by the JWL EOS. Regardless of the reaction mode, the reactants were represented by the JWL reactant EOS. This EOS was substituted into the ViscoSCRAM material model in place of the simple linear bulk modulus based EOS previously implemented. Section 2.2 has further discussion on the ViscoSCRAM implementation.

2.2. Material Models

Bennett presented a model for statistical treatment of cracks in a bulk volume of viscoelastic material and called it ViscoSCRAM [19]. Advantages of this model include the ability to evolve average cracking without predefined boundaries or advancement of the state of such boundaries as other crack models do, making it suitable for use in UCF where boundaries are not well defined. ViscoSCRAM takes an initial crack size, maximum crack growth rate, several other crack rate parameters and five Maxwell elements, each including a modulus and related relaxation time. From these, average crack size is evolved from a balance between crack coalescence and separation. PBX 9501 calibrated parameters from Bennet et al were used

[19]. Average crack size is used in the threshold criteria for onset of convective burning into cracks, as will be discussed in Section 2.3. A bulk modulus of 11.4 GPa was used as it is an often cited literature value [20].

Oxygen-free high conductivity copper was used as the encasing material in the Cylinder tests. Since the velocity of the copper is the data of interest in these simulations, accurate representation of the material is paramount. A compressible Neo-Hookean stress relationship was used, with standard bulk and shear moduli. A yield stress of 70 MPa and a hardening modulus of 4.38 μ Pa were used. A thermal conductivity of 400 W/mK and a specific heat of 386 J/kgK were used.

During Pop plot simulations, 6061-T6 aluminum was used as the impactor and cover plate, and was the only non-reactant material of relevance in the simulation. Standard shear and bulk moduli were used along with a Mie-Grüneisen EOS with values $C_0 = 5386$ m/s, $\gamma_0 = 1.99$ and $S_\alpha = 1.339$. A shear modulus model developed by Nadal-LePoac (NP) was used [21]. Melting was modeled with the Steinberg-Cochran-Guinan (SCG) model with parameters $T_{m0} = 2310$ K, $\gamma_0 = 1.97$ and $\alpha = 1.5$ [22]. A Hancock-MacKenzie damage model was used, with a Gurson yield condition [23, 24]. A specific heat model designed for copper was used, of the form Eq. (1) with parameters $A_0 = 4.16 \times 10^{-5}$ J/kgK⁴, $B_0 = 0.027$ J/kgK³, $C_0 = 6.21$ J/kgK², $D_0 = 142.6$ J/kgK, $A_1 = 0.1009$ J/kgK² and $B_1 = 358.4$ J/kgK where 270 K is the pivot point for the piecewise definition.

$$C_p = \begin{cases} A_0 T^3 - B_0 T^2 + C_0 T - D_0 & T < T_0 \\ A_1 T + B_1 & T \geq T_0 \end{cases} \quad (1)$$

The final material used in simulating the validation experiments was steel. A hypoelastic-plastic constitutive model with a Mie-Grüneisen EOS was used with parameters $C_0 = 3574$ m/s, $\gamma_0 = 1.69$ and $S_\alpha = 1.92$. A Johnson-Cook plasticity model was used in conjunction with a Johnson-Cook damage model, and a Gurson yield condition with the same parameters as those for copper [25, 26]. The specific heat model described by Lederman et al was used [27]. A full description of the steel, copper and aluminum material representations as well as citations for material parameters with assessment of accuracy and error can be found in the works of Banerjee [14]. Finally, a friction model developed for MPM was used for interaction between materials, generally with a frictional coefficient of 0.3 [28].

2.3. Reaction Models

Two previously validated models for the two limiting modes of combustion were used in DDT1. Combustion in both surface burning and bulk convective burning regimes were represented by WSB reaction model [4]. This model had previously been implemented in UCF as a 3D model, named Steady Burn, by including a surface area calculation based on the direction of density gradient in the cells and the total mass of reactant in that cell [5]. Surface detection for surface burning and density gradient require MPM materials, hence the reason MPMICE is used. PBX 9501 parameters can be found in literature [4, 5]. Transition

from surface burning, where only the top cell of the surface is allowed to burn, to convective burning, where the burning front penetrates into the material, is determined by Eq. (2), a relationship described and fit by Berghout et al and proposed by Belyaev et al [29, 30].

$$p_c^{1+2n} w^2 = p_c^{2.84} w^2 = 8 \times 10^8 \quad (2)$$

When the pressure in a cell exceeds the critical pressure for propagation of flames into cracks, p_c , determined from the average extent of cracking, w , calculated by ViscoSCRAM, bulk burning occurs. In addition to this requirement, the gas in the cell must be above the melting and thermal runaway temperature for the explosive; 450 K in the case of PBX 9501 [31]. This allows burning in damaged material (i.e. cracked or porous) ahead of the deflagration wave without any sub-grid scale models for hot spots or shear heating. Good agreement has been obtained with a variety of experiments that exhibit convective burning. This threshold is applicable in cook-off scenarios, where the material is heated to decomposition point over large areas of the bulk.

Detonation is carried out by a modified version of the JWL++ model [6]. Model fitting simplicity is attained by using this first-order, single term rate model, Eq. (3), as only two parameters need to be fit.

$$\frac{dF}{dt} = G \times (1 - F) \times P^b \quad (3)$$

The pressure exponent was chosen to be 1.2 and the rate coefficient $2.33 \mu\text{Pa}^{-1.2}\text{s}^{-1}$. As described elsewhere, these parameters control the size effect curvature and infinite radius detonation velocity, respectively [6, 32, 16]. Two differences exist between the JWL++ implementation by Souers et al and DDT1. First, DDT1 uses a JWL EOS for reactants instead of the Murnaghan EOS. The decision to use the JWL equation of state was made as a consequence of the zero experienced by the Murnaghan EOS at relative volume equal to 1.0 and subsequent “negative pressure” during expansion beyond initial state—a common occurrence for viscoelastic materials undergoing large relaxation. Negative pressures cause exceptions to be thrown in Uintah². As mentioned, parameters from Vandersall et al were used as they had been found to give good detonation and CJ behavior with Ignition and Growth [17]. Second, instead of additive pressure, the built in iterative pressure solve in ICE is used to correct for the simple Dalton’s law assumption in its original formulation.

A transition mechanism in the form of a pressure threshold acts as the link between burning and detonating. The models are mutually exclusive, only burning or detonating is allowed in any given cell at a time. Furthermore, burning is prevented in cells adjacent to detonation, as this sort of burning was found to accelerate the shock wave unphysically. Once the pressure threshold is exceeded, the detonation begins.

²Negative pressures are considered nonphysical and are disallowed in the equilibration step of the pressure in a cell in the ICE component of MPMICE

Equilibrium cell pressure has mixed contributions from stresses of all MPM materials and the cell centered pressures for each ICE material. However, the primary functionality of ViscoSCRAM is turned off in a cell undergoing detonation to minimize computation leaving stress to be simply calculated from the reactant JWL equation of state. For PBX 9501, 5.3 GPa was chosen as the threshold.

3. Results and Discussion

3.1. Surface Regression

Surface regression rate, reported as a velocity, is the rate the propellant is consumed normal to the burning HE surface. This velocity is used as the primary metric for validation of combustion in both the convective burning and surface burning regimes. This is possible due to regression rate measurements up to the regime where surface burning will propagate into cracks on the order of the average size in pristine PBX material [33, 34]. Strand burner apparatuses, diagramed in Fig. 2 of Atwood et al, are generally used for velocity measurements as they are able to measure the burn rate over a range of pressures using one burn sample as it pressurizes the apparatus [33]. One sample is fired for each bulk temperature of interest. Several surface regression rate studies have been performed covering a large pressure range, approximately 0.24 to 345 MPa and four initial bulk temperatures [33]. Measurements were performed so that a 1D simulation with symmetric boundaries on non-principle faces should suffice for model comparisons.

Simulation setup differs slightly from experimental in initiation as well as confinement. In order to get good burn rate measurements, an open domain was used, with a Neumann pressure boundary imposed on the open end and gas at the pressure of interest filling the non-solid partition of the domain. HE material was ignited with a localized region of gas at 600 K at and slightly above the surface of the explosive, which differs from the flash-wire ignition used in experiments. Measurements were taken after initial burn rate instability had subsided and taken as an average over the time to burn three or four computational cells completely. Unlike the Strand Burner experiments, one simulation was run at each pressure, instead of measuring the burn rate of confined explosive as the vessel pressurized.

Surface regression rates were found to generally agree in value and trend for pressures greater than around 1 MPa and less than 70 MPa. These are important ranges in DDT in confined and lightly confined scenarios [35]. For example, in pristine material where average crack size is between 2 and 25 μm , Eq. (2) translates to between 2.3 to 9.2 MPa. As seen in Fig. 1, outside these ranges, the simulated regression rate was found to deviate by as much as 2 times, though this large a magnitude difference is only seen at very low pressures and thus are only important in unconfined explosive scenarios where bulk burning is not possible. Regardless, these ranges may provide some uncertainty in a slow cook-off experiment, and more simulations are needed to quantify the uncertainty. At large pressures, simulations overestimate the burn rate by approximately 10%, twenty times the experimental error cited in Atwood et al [33].

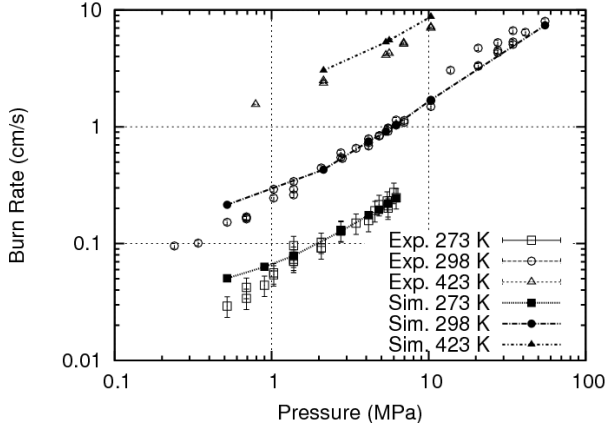


Figure 1: Simulated surface regression rates compared with experimental values. Error bars are those assigned by Atwood et al [33]. Note the range of good agreement are those typical of convective burning, suggesting application to those scenarios is reasonable. Values for both experimental and simulations at high and low temperatures have been multiplied and divided by 4 respectively, for clarity.

Bulk temperature simulated burn rate dependence, seen in Fig. 2, is overestimated for low and high temperatures. Overestimated rates are especially pronounced at high pressures. Again, this could cause issues in slow cook-off simulations. Generally, in SDT situations, the bulk temperature of the material is near room temperature and the shock itself does not raise the temperature of solid HE high enough, long enough to initiate bulk thermal reaction. However, small hotspots created through impedance mismatch, crack and surface interaction friction, and other dissipative mechanisms create high pressure/temperature reactive gases in the material that then propagate through cracks [36, 34].

Convergence results for the burn rate with varied cell resolution can be seen in Fig. 3. An intermediate parameter simulation was used for convergence, that of the 6.21 MPa pressure and 298 K bulk temperature. The burn rate converges at higher zonings per millimeter. As can be seen in the figure, the convergence is fast for resolutions higher than 1 zone/mm, though the converged value is about 7% larger than the averaged experimental value of 1.089 ± 0.077 cm/s. Relaxation to steady burning state is a function of the cell size. As a result, the uncertainties are likely to be larger than those we present shortly. Figure 3 shows time to steady state as a function of resolution. At low zoning per millimeter the trend indicates the time for DDT may be skewed due to overestimated burn rate during ignition and subsequent move towards stabilization, an effect that may require a larger model pressure threshold for transition to detonation than experimentally determined [37].

Particle density was varied from 2 cubed to 6 cubed per cell and had negligible effect on the burn rate. Because the Steady Burn implementation only uses cell centered values for computation of the actual burn rate, no particle density dependence was expected. At 2, 3, 4 and 6 cubed particles per cell, the burn rates differed by a maximum of 0.02% over a factor of 27 times higher particle resolution, and this can be attributed to round off errors in the cell centered mass during particle interpolation to the grid and

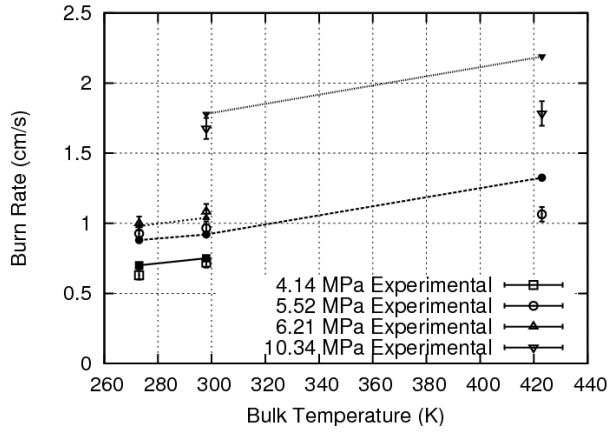


Figure 2: Simulated temperature dependence shown by connected points. Error bars are those assigned by Atwood et al [33]. Note that too high a bulk temperature will generally cause burn rate to be overestimated in simulation, meaning that cook-off transition to detonation occurs too early.

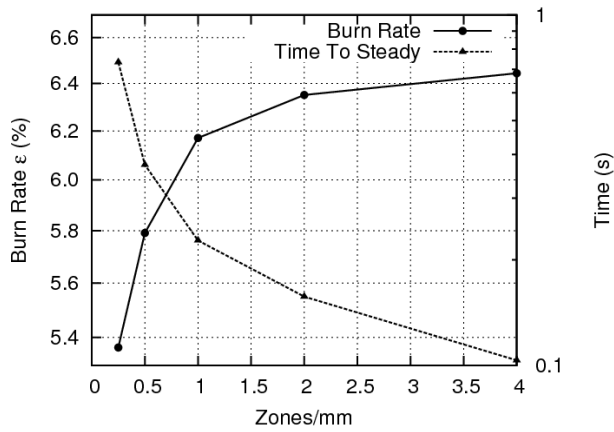


Figure 3: Burn rates are shown to converge at finer resolution. The burn rate converges to an error near 6.5% larger than the experimental value. On the right axis is shown the time to steady state burning for the different resolutions. The right axis is plotted on a log scale.

subsequent averaging to give the cell centered values.

Comparing errors between simulated and experimental values in Fig. 2 give standard deviations of 0.061, 0.072 and 0.483 cm/s for low to high temperatures, consistent with 7.2, 6.5 and 27.1% error. A weighted average of these uncertainties gives a value of 6.04%. As previously mentioned, low bulk temperatures give reasonable uncertainty, with reasonable uncertainty being quantified as less than 10%. Also as mentioned before, huge error is found at high initial bulk temperatures, introducing large uncertainty into any slow-cookoff simulations.

Errors calculated over the full pressure range at 273, 298 and 423 K were computed. Uncertainties on the average of 6.56%, 3.17% and 20% were found for the cases. A weighted average gave 4.42 %. These values are similar in trend to those just mentioned for temperature dependence, and indicate that simulations performed with bulk temperature near room temperature should give less than 7% uncertainty during burning.

3.2. Detonation

Detonation characteristics were determined from the Pop-plot simulations. Reaction front velocity and Chapman-Jouguet pressures are the two qualities of interest in detonation, both of which are readily available from the 889 m/s impact. See Section 3.5 for behavior of different impact velocities. Pop-plot tests are one dimensional SDT experiments, first designed by Popolato and designated the “Plane Impact Test.” Both low and high impact pressure regimes have been studied [17, 15]. Simulation setup includes a one dimensional domain with device geometry described in Vandersall et al, 2010 [17]. In simulation, an aluminum impactor is initially in contact with an aluminum cover plate confining 45 or 90 mm of PBX-9501 disks along the principle axis of the simulation. Symmetry boundaries are applied to the non-principle faces to mimic measurements at the center of the cylinder where strong confinement was emulated in the experiments.

Parameters were found that match both detonation velocity and detonation pressure at the resolution used for calibration. Values of 1.2 for b and $2.33 \mu\text{Pa}^{-1.2} \text{s}^{-1}$ for G in Eq. (3) were found to give reasonable values. The detonation velocity at this resolution was found to be 8843 m/s and the detonation pressure was found to be 37.2 GPa. Detonation Chapman-Jouguet pressure is overestimated; however this has already been identified by Menikoff as a consequence of the EOS fits [38]. Resolution effects were explored for the same resolutions studied for the Strand Burner simulations.

Particle resolution dependence was studied at 4 zones/mm cell resolution, as this was the calibration resolution. Results are presented in Fig. 4. Detonation pressure error was found to decrease with greater particle resolution, relative to the 37.2 GPa at 8 particles per cell. However this effect is small, with the error decreasing by only a factor of two over 27 times higher particle density. Detonation velocity error, however, increased with higher particle resolution relative to the 8.870 mm/ μs cited in literature. In fact, increasing the density of particles by 27 times increases the error from about 0.04 mm/ μs to as high as 0.221

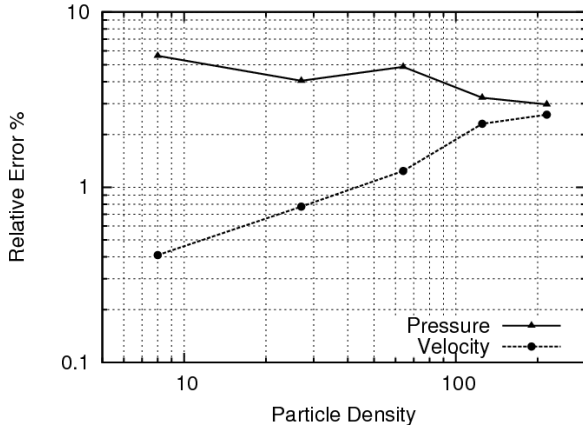


Figure 4: Particle density dependence of CJ pressure and detonation velocity. Values are varied from 8 to 216 particles per cell. Both axes are logscale.

mm/ μ s. These effects are small in the terms of overall simulation error already cited, which generally fell in the range of 5 to 10%. In fact, the relative error in all cases studied for both velocity and pressure were less than 6%. Due to these conflicting resolution effects, the particle resolution should be limited to between 2 cubed and 4 cubed particles per cell for the reactant.

Cell resolution has a considerably more noticeable effect on detonation pressure and velocity, see Fig. 5. Intuitively, this is because the model itself uses cell centered (i.e. ICE) variables in determining masses of the various materials in the cell. Convergence in detonation velocity was found to be strong, while convergence of detonation pressure less-so. The values are converged to within 5% relative simulation error at resolutions lower than the calibration resolution 4 zone/mm but greater than 0.5 zones/mm. Detonation velocities quickly diverge at coarser zoning. Simulations run must be at least 4 zone/mm for accurate detonation. Chapman-Jouguet pressure for the explosions were found to follow a less favorable trend, with unexpected behavior at low zoning. At low resolution, the pressures were found to be underrepresented, with normal convergence behavior found at finer zoning. Low resolution runs are so far from the size of the actual reaction zone that the detonation pressure is weakened by the overrepresentation of reaction zone width which is the size of the cell in these low resolution, engineering simulations.

3.3. Case Expansion Velocity

Validity of the JWL equation of state for product expansion can be tested by simulating an explosion propagating down a cylindrical tube. The Cylinder test measurements are used for calibrating product gas equations of state [39]. A cylinder test geometry schematic for the standard 1 inch test can be seen in Catanach et al [40]. Case expansion velocity as a function of case expansion distance from initial radial position is the primary metric. From x-ray measurements, the density at and just behind the reaction zone is measured, which is converted to a characteristic starting volume which can be used to determine

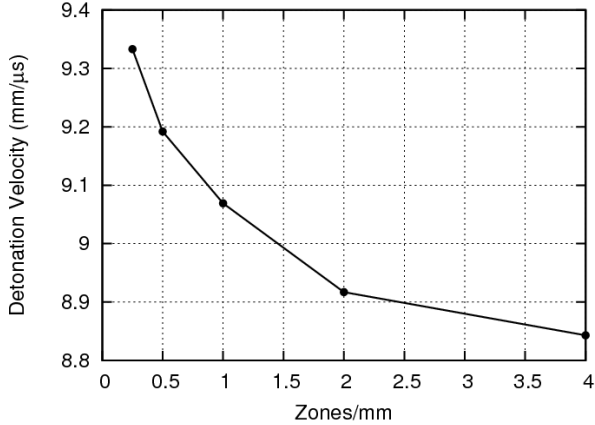


Figure 5: Cell Resolution dependence of the detonation velocity shows that 2 to 4 zones/mm are close to the edge of convergence for the JWL++ model.

subsequent expansion volumes [41]. These two bits of information can be used to construct a pressure versus relative volume plot, that is used to calibrate an expansion isentrope, of use in a pressure/density model like MPMICE. Similarly, the velocity can be used directly to determine detonation energy, which could also be used to calibrate energy based models from elsewhere [42, 38]. Our simulations model the copper cylinder and the explosive in 3D with quarter symmetry (two orthogonal symmetry planes down the axis of the cylinder). Measurements were taken at least 9 times the diameter down the axis of the tube from the initiation point, as suggested by Souers et al [43].

Case expansion velocity at 2 zones/mm resolution was used as a benchmark and a screenshot of the test can be seen in Fig. 6. This simulation consisted of 5.3 million grid cells and 12 million particles. During simulation the CJ pressure at the front reached 37.12 GPa, in good agreement with detonation pressure presented in the previous section. Comparison of simulated data and an experimental data set from Gibbs et al are seen in Fig. 7 [39]. Of note is the overestimation of case expansion at low expansion volumes (early times), potentially due to the overestimation in CJ pressure. This is consistent with the overestimation of CJ pressure due to a fitting form that is too stiff for PBX 9501 [38]. An error between 6.3 and 7.8% can be found as a standard deviation between simulated and experimental velocity profiles. This is roughly equivalent to 0.12 mm/μs. Again, this value is below 10% and thus should be considered as good for simulations. Note, however, the good agreement at high expansion volumes. Expansion velocities at large distances are of interest in DDT scenarios as personnel affected by the incident will likely be far from the explosion. Overestimation of explosive violence should be expected in packed arrays of explosives or where explosives are in close proximity to one another.

Particle density dependence of detonation velocity and pressure in the Cylinder test simulations are similar to those presented under the symmetrically bound detonation test presented in Section 3.2 though slightly less pronounced. The detonation velocity varied by only about 0.2% and the detonation pressure

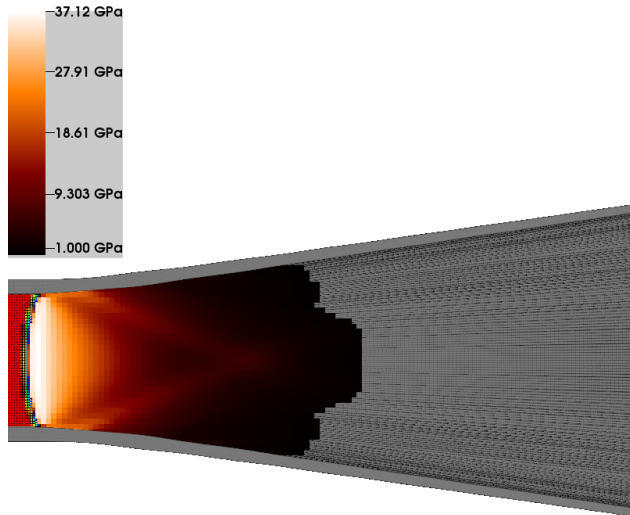


Figure 6: An image from the simulation of the 1 inch Cylinder test shows case expansion in gray. Pressure is cutoff below 1 GPa and the values are represented by the scale bar. The curved reaction front can also be seen, at the interface between MPM reactant material and ICE product material.

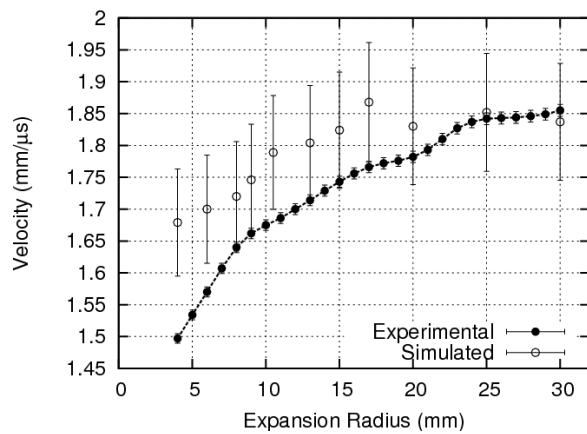


Figure 7: Case expansion comparing simulated and experimental data [39]. Agreement is good for large case expansion, while overestimated near beginning of expansion due to the stiff EOS fit.

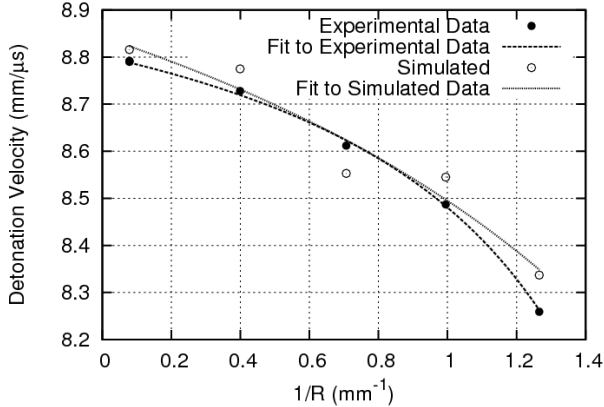


Figure 8: Simulated and experimental size effect curves for PBX 9501.

varied by about only 1.3%. Case expansion velocity varied by a maximum of 3.7% over the range of particle resolutions studied.

3.4. Failure Diameter

Size effect curves are indicative of explosive performance as they are related to the reaction zone thickness [44]. Larger reaction zones cause failure on larger length scales (of the order of millimeters to centimeters). On length scales slightly larger than failure, the detonation velocity is greatly reduced due to curvature of the reaction front, or put differently, the explosive violence is dampened due to inertial effects, in the case of unconfined explosives. The general behavior of explosives has been found to follow: $D(r) = D(\infty)(1 - A/(r - r_c))$, where A and r_c are fit parameters. Rate stick experiments have been performed for PBX 9501, however the extent of data is somewhat limited compared with other composite explosives [39]. The simulation is run with the same input file as the Cylinder test with the copper casing removed and at varied explosive radii.

Simulated detonation velocity versus inverse radius can be seen in Fig. 7 extending to infinite radius detonation velocity already discussed in Section 3.2. A fit to the simulation data yields $D(d) = 8.843\text{mm}/\mu\text{s} \times (1 - (0.028\text{mm} \pm 0.009\text{mm}) / (r - 0.29\text{mm} \pm 0.19\text{mm}))$. Extrapolating to intersection with the inverse radius axis gives a failure diameter (d_f) of 0.70 mm. This is consistent with the experimental value cited in LASL Explosive Property Data, $d_f < 1.52$ mm, which is of little certainty, as they never achieved failure with PBX 9501 charges [39]. Experimental fit parameters are $D(\infty) = 8.802$ mm/μs, $A = 0.019$ mm \pm 0.001 mm and $r_c = 0.48$ mm \pm 0.02 mm and lie on the edge of uncertainty of the simulation fit parameters. Differences in the infinite radius detonation velocities likely contribute to much of the difference in fit parameters.

A simple addressing of error between experimental and simulated results gives a standard deviation for simulations of 0.063 mm/μs, which is equivalent to about 0.7% total velocity. This is likely a very

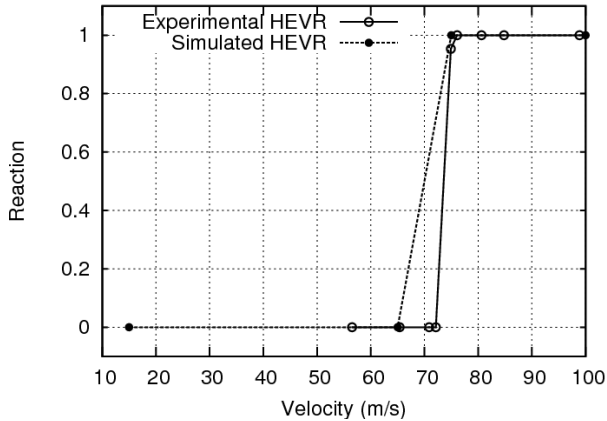


Figure 9: Go/no-go simulated and experimental results. Violent reaction as defined is used to determine a “go” and represented by a 1 in the plot [47].

optimistic value but nonetheless indicates that the detonation velocity over various explosive sizes are well represented. Assumed, in this analysis, however, is running a simulation at a converged zoning, and errors likely increase as resolution is coarsened. No resolution studies were performed for the failure diameter simulations. From an input specification standpoint, the Cylinder test is the parent of the rate stick test, and the particle resolution dependence is similar. Furthermore, the effect of cell resolution on detonation velocity has already been presented, of which the rate stick test should closely follow.

3.5. LANL Modified Steven Test

The Steven Test is perhaps the most complicated experiment designed for explosive model validation [45]. Similarly, in simulation, this is the most expensive test, consisting of 66.5 million cells and 15.6 million particles. A lightly confined disk of PBX 9501 is impacted with a round nosed projectile and stress histories are measured. From this test, a velocity threshold is determined for go/no-go behavior where “go” implies rapid, sustained reaction. Go/no-go is a basic metric for explosive impact assigned based on reaction of the sample. Sometimes another set of terms: nonviolent, semi-violent and violent, are used to describe the test behavior. Cracking and damage to the material are exhibited in all velocity impacts and are not used as the go/no-go criteria. Instead, consumption of large amounts of target material along with melting and scorching are used to assign the go/no-go label. In simulation, pressure in the vessel never exceeds 5.3 GPa indicating detonation was not achieved, in good agreement with analysis of experiments where explosive energy releases are much lower than fully formed detonation [46].

Experiments show a threshold for large, 1 inch thick targets of approximately 72-75 m/s with cracking occurring at lower velocities, and target consumption at higher velocities than the threshold. A stress threshold of approximately 250 MPa follows from 75 m/s experimental case for rapid reaction, indicating a lower threshold to dissipation of energy. Figure 9 shows simulated versus experimental go/no-go results.

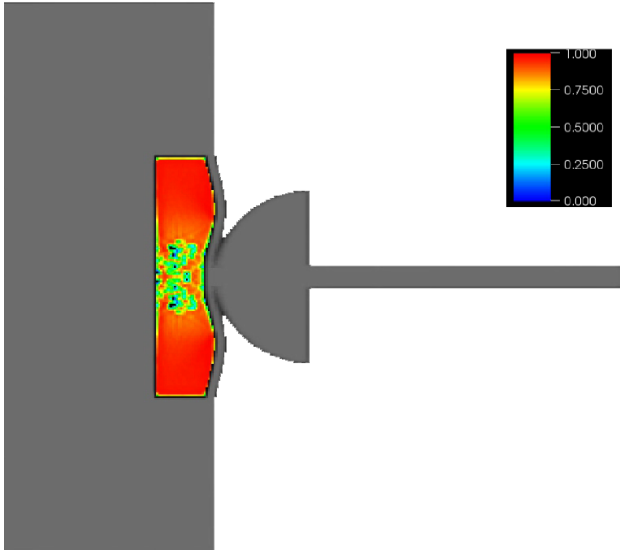


Figure 10: A steel enclosure, with a hockey puck shaped cavity containing a disk of PBX 9501, is impacted by a round nosed steel projectile at 75 m/s. Reaction begins at roughly a 45 degree angle from the centerline, and grows as a set of reacting pockets or “hot spots”.

Good agreement was found between DDT1 and experiments, indicating decent burn initiation behavior. Pinducer traces of the experiments qualitatively match simulated pressure profiles at the same point in the explosive, especially with regards to timescales of material response, but magnitudes differ by as much as three times. Inconsistencies have been attributed to MPMICE’s failure to handle negative pressures. Figure 10 shows reaction beginning in the 75 m/s case.

3.6. POP Plot

Pop plot setup was discussed in Section 3.3. Run distance to detonation is important metric of shock sensitivity [39]. Buildup to detonation is due largely to nucleation and growth of hotspots, as well as other dissipative mechanisms such as frictional heating between cracks and resultant bulk decomposition due to expansion of hot product gasses through cracks effectively increasing burning surface area and in turn the rate of reaction. Support and strengthening of the lead front results, eventually providing enough available energy for rapid transition to detonation. A pressure threshold of 5.3 GPa was used for transition from deflagration to detonation in simulations, a value that roughly represents the amount of work necessary for rapid reaction in the bulk explosive.

Figure 11 shows the Pop plot for simulations and experiments. Though the simulations were run with 1.832 g/cm³ density, the Pop trend is found to lie closer to the 1.844 g/cm³ experiments from LASL in magnitude [39]. Of particular note, however, is the slope of the trend, which is in between the two density trends cited for experiments. These facts indicates that in general the model is not as dependent on density as it should be. A rationale for this threshold from a work energy perspective is presented in Section 3.7.

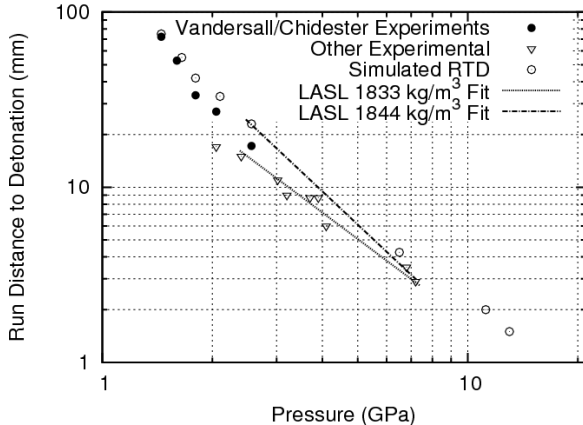


Figure 11: Pop plot for simulation of 1.832 g/cc PBX 9501. Note general trend is close to experimental results over a wide range of pressures. Experimental data comes from Vandersall et al [17]. Other experimental data and fits from Gibbs et al and Gustavsen et al [39, 48].

3.7. Extended Discussion

Of largest uncertainty in the model is the pressure threshold chosen to transition from deflagration to detonation. Thermodynamically, the activation of HMX reaction requires average energy in the range of 140 to 165 kJ/mol [49]. Bulk reaction should occur when the entire material within a given volume has exceeded this energy, which will result in fast reaction and large energy buildup. The pressure threshold of 5.3 GPa in this model was chosen for two reasons. First, the threshold was chosen so that the 351 m/s aluminum impact experiment gave a reasonable run distance to detonation. This likely increased the threshold value above what it might be in reality due to overestimation of burn rate. Second, a 2003 paper by Esposito et al shows an increase in the pressure dependence of HMX burn rate from 0.924 to 1.27 at about 5 GPa. And while these experiments were performed at ambient temperature instead of in a reactive flow state, no other simple combustion measurements on HMX have been reported at these pressures. In real scenarios, hot spots and the resulting convective burning in porous voids are of great importance to conductive burning, but here we model on the bulk scale. WSB has a pressure dependence of approximately 0.9 at low pressures and the pressure dependence of the detonation model calibrated herein show reasonable size effect at a pressure dependence of 1.2, indicating that there is good agreement with this experimental data.

A simple mathematical analysis of the energy available under compression to 5.3 GPa leads to perhaps more understanding. Transition state theory supplies an equation, $k \propto \exp(\Delta\dagger S/R)\exp(\Delta\dagger H/RT)$, in which the entropy, if isothermal, reversible work is assumed, can be altered to $\Delta S = PdV/T$. This analysis would imply that a certain amount of work could be analogous to raising the material to the temperature of ignition. Using a simple expression $P = K/2 \times (1/v - v)$, where v is the relative volume, the bulk modulus, K , is 11.4 GPa and HMX has an approximate molar volume of 6200 mols/m³, one comes to an average energy of compression of 138.9 kJ/mol. Surprisingly this value is close to the experimental activation energies.

Using an upper bound of experimental bulk moduli for HMX reported in literature of 15.7 GPa the same analysis leads to a slightly lower value of 119.4 kJ/mol available energy [50]. Since the bulk modulus of PBX 9501 is lower than HMX due to the plasticizer, the higher energy result first discussed may be more reasonable. This equation of state assumes isothermal compression, which is not necessarily the case in shocks, and thus deviates from experimental compression measurements after compressions to about 0.85 initial volume. As a check we apply the same analysis with the shock EOS. Using the JWL equation of state for reactants, which fits the experimental data up to $v = 0.8$ fairly well, and the afore mentioned molar volume, the available energy is much lower, around 45.2 kJ/mol. As another check we should try using a different pressure threshold. Doing this analysis at lower pressure threshold, say 3.0 GPa leads to the much lower average energies of 53.1 kJ/mol and 22.3 kJ/mol for the simple and JWL equation of states, respectively. However, since a shock wave is generally sharper than the cell width in simulation, these values may be low due to bulk averaging over the cell volume and the energy available to a shock front may be higher than these averaged values.

Some drawbacks and uncertainties are associated with using DDT1. Firstly, the calibration of JWL++ rate parameters are required after a factor of 8 coarser zoning, as the reaction zone becomes over-represented and the errors in detonation pressure and velocity are greater than 5%, which seems to be the reasonable value for simulations. Souers et al has already covered this issue in several of their papers [6, 16]. What this means for a simulation framework such as Uintah in which Adaptive Mesh Refinement (AMR) is used, is that the detonation should be resolved at the finest level of AMR to at least 2 times coarser zoning than the calibration resolution, and preferably the calibration resolution. Secondly, there has been some uncertainty regarding the actual convergence of the JWL++ model [51]. However, this has been identified as an issue with additive pressure approaches to equilibrium. Thirdly, as was just discussed briefly, a constant value for a pressure threshold is subject to much uncertainty, due in part to the fact that this initiation pressure is dependent on explosive density [37].

A fourth drawback comes from the WSB model. Particularly, few explosives have all the experimentally determined observables necessary to run the model. Such values as chemical heat release for gas condensed phase, the specific heat of both gas and solid, and condensed phase activation energy have been identified as the sensitive parameters of the model and thus need to be known to high certainty from experiments [4]. Furthermore, the time to steady state burning in the model likely has a large effect on transition to detonation.

Along a similar note, one final drawback is the limited experimental data available for calibrating the ViscoSCRAM model for cracking behavior. And to the authors' knowledge no data regarding propagation of surface flames into cracks is available for explosives other than PBX 9501. Luckily, these experimental parameters are probably much more similar between explosives than burning parameters, and thus the models should be applicable within a quantitative sense, for other explosives. However, lack of complete

sets of 1D, 2D and 3D experiments for many explosives other than PBX 9501 make validating the model for other explosives nigh impossible.

The simulation methodology provided herein, which is supported by the functionality of UCF, should be noted as a success. The ability to rapidly prototype a simulation with relatively simplistic material models, and then layer on complexity makes running a full suite of validation simulations for a model feasible. Furthermore, the rapid development time for models that are plug-and-play as well as the scalability of the platform from 1 CPU to the total available processors on the largest super computers provides a simulation framework robust enough to handle any size problem from rapid turn around to full fledged validation studies with no extra knowledge or training required [8, 9].

4. Conclusions

In general, the fact that semi-empirical models can be mixed with empirical models, is an excellent proof of concept. Several current models have the ability to do SDT, including Lee and Tarver's Ignition and Growth model [52], WSD model [53] and CREST model [54], however all are designed as purely empirical in the regime of convective burning/hot spot initiation. There has been work recently in providing semi-empirical models for ignition of explosives under stresses, including work by Dienes et al using SCRAM and Reaugh et al's model for initiation [55, 56]. However, to our knowledge, this is the first model that uses a semi-empirical model for the point between ignition and detonation; the entire regime of convective burning.

This indicates that merging two models with vastly different scopes, such as WSB and JWL++, and a few experimentally derived thresholds inside a physics framework can have true utility. Furthermore, the surprisingly good agreement between simulations and experiments indicates that the mechanism assumed herein for convective burning has some merit. More generally, the idea is that hot gas at high pressures can flow through the voids in an explosive, causing more rapid reaction. Relating this to the normal factors cited as causing DDT such as frictional heating, hotspot nucleation and growth, shear and heating of solid near hot cavity gases, leads to the startling conclusion that all of these phenomena can be related to the simple process of hot gas flowing through a solid. Menikoff has recently discussed how reacting gas mixing with solid can greatly increase reaction rate further validating this conclusion [57].

Several modifications to the model could be performed to extend the range of applicability. One would be implementation of Souers' two term JWL++ model for less ideal explosives [32]. Another would be implementation of modified JWL equation of state mentioned by Tang for better overdriven detonation product prediction [58]. Of particular interest would be a validation against one of the DDT Tube tests performed at LANL and annular confined cook-off experiments. Finally, a porous media flow model should be implemented and calibrated with experimental evidence, to further test the theory of the role of flowing reactive gases. Ongoing work is currently being manifested in a DDT2.

5. Acknowledgements

This work was supported by the National Science Foundation under subcontract No. OCI0721659. The authors would like to thank the whole University of Utah's Center for Simulation of Accidental Fires and Explosives (C-SAFE) team of software engineers, computer scientists and application scientists. The authors acknowledge the Texas Advanced Computing Center (TACC) at The University of Texas at Austin for providing HPC resources that have contributed to the research results reported within this paper. URL: <http://www.tacc.utexas.edu> An allocation of computer time from the Center for High Performance Computing at the University of Utah is gratefully acknowledged. JRP would like to specially thank Todd B. Harman and James E. Guilkey for invaluable help and guidance in running and modifying UCF.

- [1] P. Dickson, B. Asay, B. Henson, and L. Smilowitz *Proc. R. Soc. Lond. A*, vol. 460, pp. 3447–3455, 2004.
- [2] K. Kline, Y. Horie, J. Dick, and W. Wang *Shock Compression of Condensed Matter*, pp. 411–414, 2001.
- [3] J. de St. Germain, J. McCorquodale, S. Parker, and C. Johnson in *Ninth IEEE International Symposium on High Performance and Distributed Computing.*, (IEEE, Piscataway, NJ), pp. 33–41, 2000.
- [4] M. Ward, S. Son, and M. Brewster *Combust. Flame*, vol. 114, pp. 556–568, 1998.
- [5] C. Wight and E. Eddings *Advancements in Energetic Materials and Chemical Propulsion*, vol. 114, pp. 921–937, 2008.
- [6] P. Souers, S. Anderson, J. Mercer, E. McGuire, and P. Vitello *Propell. Explos. Pyrot.*, vol. 25, pp. 54–58, 2000.
- [7] J. Guilkey, T. Harman, and B. Banerjee *Comput. Struct.*, vol. 85, pp. 660–674, 2007.
- [8] M. Berzins, J. Luitjens, Q. Meng, T. Harman, C. Wight, and J. Peterson in *Proceedings of the Teragrid 2010 Conference*, (Pittsburgh, PA, USA), August 2010.
- [9] J. Luitjens. PhD thesis, University of Utah, 2010.
- [10] A. Amsden and F. Harlow *Comput. Method. Appl. M.*, vol. 3, p. 80, 1968.
- [11] D. Sulsky, Z. Chen, and H. Schreyer *Comput. Method. Appl. M.*, vol. 118, pp. 179–196, 1994.
- [12] S. Bardenhagen and E. Kober *Comp. Model. Eng. Sci.*, 2006.
- [13] P. Wallstedt and J. Guilkey *Comp. Model. Eng. Sci.*, vol. 19, no. 3, pp. 223–232, 2007.
- [14] B. Banerjee *Int. J. Solids. Struct.*, vol. 44, no. 3-4, pp. 834–859, 2007.
- [15] S. Chidester, D. Thompson, K. Vandersall, D. Idar, C. Tarver, F. Garcia, and P. Urtiew *Shock Compression of Condensed Matter*, vol. 955, pp. 903–906, 2007.
- [16] P. Souers, R. Garza, and P. Vitello *Propell. Explos. Pyrot.*, vol. 27, pp. 62–71, 2002.
- [17] K. Vandersall, C. Tarver, F. Garcia, and S. Chidester *J. Appl. Phys.*, vol. 107, 2010.
- [18] C. Twu, V. Tassone, W. Sim, and S. Watanasiri *Fluid Phase Equilibr.*, vol. 228-229, pp. 213–221, 2005.
- [19] J. Bennett, K. Haberman, J. Johnson, B. Asay, and B. Henson *J. Mech. Phys. Solids*, vol. 46, no. 12, pp. 2303–2322, 1998.
- [20] J. Dick, A. Martinez, and R. Hixson in *11th Int. Symp. On Detonation*, (Snowmass, CO, USA), pp. 317–324, 1998.
- [21] M. Nadal and P. L. Poac *J. Appl. Phys.*, vol. 93, no. 5, pp. 2472–2480, 2003.
- [22] D. Steinberg, S. Cochran, and M. Guinan *J. Appl. Phys.*, vol. 51, no. 3, pp. 1498–1504, 1980.
- [23] J. Hancock and A. MacKenzie *J. Mech. Phys. Solids*, vol. 24, pp. 137–167, 1976.
- [24] A. Gurson *ASME J. Engg. Mater. Tech.*, vol. 99, pp. 2–15, 1977.
- [25] G. Johnson and W. Cook in *Proc. 7th Int. Symp. on Ballistics*, pp. 541–547, 1983.
- [26] G. Johnson and W. Cook in *Int. J. Eng. Fract. Mech.*, vol. 21, pp. 31–48, 1985.
- [27] F. Lederman, M. Salamon, and L. Shacklette *Phys. Rev. B*, vol. 9, no. 7, pp. 2981–2988, 1974.
- [28] S. Bardenhagen, J. Guilkey, K. Roessig, J. Brackbill, W. Witzel, and J. Foster *Comput. Model. Eng. Sci.*, vol. 2, pp. 509–522, 2001.
- [29] H. Berghout, S. Son, L. Hill, and B. Asay *J. Appl. Phys.*, vol. 99, 2006.
- [30] A. Belyaev and V. Bobolev, “Transition from deflagration to detonation in condensed phases,” *National Technical Information Service, Springfield, VA, Trans.; original work published in 1973.*, 1975.
- [31] B. Henderson, L. Smilowitz, B. Asay, M. Sandstrom, and J. Romero, “An Ignition Law For PBX 9501 From Thermal Explosion to Detonation,” in *13th Int. Symp. on Detonation*, (Norfolk, Virginia, USA), July 2006.
- [32] P. Souers, J. Forbes, L. Fried, W. Howard, S. Anderson, S. Dawson, P. Vitello, and R. Garza *Propell. Explos. Pyrot.*, vol. 26, pp. 180–190, 2001.
- [33] A. Atwood, T. Boggs, P. Curran, T. Parr, D. Hanson-Parr, C. Price, and J. Wiknich *J. Propul. Power*, vol. 15, pp. 740–747, 1999.
- [34] H. Berghout, S. Son, C. Skidmore, D. Idar, and B. Asay *Thermochim. Acta*, vol. 384, pp. 261–277, 2002.
- [35] D. Wiegand in *APS Shock Compression of Condensed Matters*, 1999.
- [36] R. Menikoff tech. rep., LA-UR-10-04480, Los Alamos National Laboratory, Los Alamos, NM 875454, July 2010.
- [37] P. Souers and P. Vitello *Propell. Explos. Pyrot.*, vol. 32, no. 4, pp. 288–295, 2007.
- [38] R. Menikoff tech. rep., LA-UR-06-2355, Los Alamos National Laboratory, Los Alamos, NM 875454, March 2006.
- [39] T. Gibbs and A. Popolato, eds., vol. 1 of 1. Berkeley: University of California Press, 1980.

- [40] R. Catanach, L. Hill, H. Harry, E. Aragon, and D. Murk tech. rep., LA-13643-MS, Los Alamos National Laboratory, Los Alamos, NM 875454, October 1999.
- [41] S. Son, B. Asay, and J. Bdzil in *APS Shock Compression of Condensed Matters*, (Seattle, WA), pp. 441–444, 1995.
- [42] L. Hill and R. Catanach tech. rep., LA-13442-MS, Los Alamos National Laboratory, Los Alamos, NM 875454, July 1998.
- [43] P. Souers, B. Wu, and J. C. Haselman Tech. Rep. UCRL-ID-119262 Rev 3, Lawrence Livermore National Laboratory, February 1996.
- [44] A. Dremin. Springer, 1999.
- [45] D. Idar, R. Lucht, J. Straight, R. Scammon, R. Browning, J. Middleditch, J. Dienes, C. Skidmore, and G. Buntain in *11th Int. Det. Symp.*, 1998.
- [46] D. Idar, R. Lucht, R. Scammon, J. Straight, and C. Skidmore Tech. Rep. LA-13164-MS, Los Alamos National Laboratory, January 1997.
- [47] C. Tarver and S. Chidester *J. Press. Vess.-T. ASME*, vol. 127, no. 1, pp. 39–48, 2005.
- [48] R. Gustavsen, S. Sheffield, R. Alcon, and L. Hill in *12th Int. Symp. on Detonation*, (San Diego, CA), pp. 530–537, August 2002.
- [49] A. K. Burnham and R. Weese in *36th Intl. ICT Conf. and 32nd Int. Pyrotechnics Seminar*, (Karlsruhe, Germany), June-July 2005.
- [50] M. Li, W. Tan, B. Kang, R. Xu, and W. Tang *Propell. Explos. Pyrot.*, vol. 35, pp. 379–383, 2010.
- [51] C. Kiyanda. PhD thesis, University of Illinois at Urbana-Champaign, 2010.
- [52] E. Lee and C. Tarver *Phys. Fluids*, vol. 23, pp. 2362–2272, 1980.
- [53] B. Wescott, D. Steward, and W. Davis *J. Appl. Phys.*, vol. 98, 2005.
- [54] C. Handley in *13th Int. Symp. on Detonation*, (Norfolk, Virginia, USA), July 2006.
- [55] J. Dienes, Q. Zuo, and J. Kershner *J. Mech. Phys. Solids*, vol. 54, pp. 1237–1275, 2005.
- [56] J. Reaugh tech. rep., LLNL-TR-405903, Lawrence Livermore National Laboratory, 7000 East Avenue, Livermore, CA, 94550, August 2008.
- [57] R. Menikoff, “Pore Collapse and Hot Spots in HMX,” in *APS Shock Compression of Condensed Matter*, (Portland, OR, USA), July 2003.
- [58] P. Tang in *APS Shock Compression of Condensed Matters*, (Amherst, MA), September-August 1997.